THE SOCIETY OF NAVAL ARCHITECTS AND MARINE ENGINEERS
601 Pavonia Avenue, Jersey City, NJ 07306
Paper to be presented at the Propellers '88 Symposium,
Virginia Beach, Virginia, September 20-21, 1988

Investigation of the SISUP (Swirl Inducing Stator Upstream of Propeller) Concept for Marine Propulsion

No. 2

T.S. Mautner, D. M. Nelson and M. C. Gillcrist, Visitors, Naval Ocean Systems Center, San Diego, CA

ABSTRACT

Except for those special applications where requirements dictate the use of counterrotating propellers, the choice between a single propeller and counterrotating propellers involves a tradeoff related to the higher efficiency of the counterrotating propellers and the greater complexity of the counterrotating machinery. The favorable effect of tangential velocity cancellation achieved by a counterrotating propeller system can be realized without counterrotating machinery by placing upstream of a propeller a stator that generates tangential velocities which are exactly canceled out by the propeller. The results of theoretical calculations show that, using the single propeller as a baseline, the increase in efficiency for SISUP is 50% of that achieved by counterrotating propellers. The feasibility of SISUP for marine propulsion was demonstrated by the design and at-sea testing of a SISUP propulsor. The comparison of SISUP's at-sea data and design predictions shows good agreement in both propulsive coefficient and vehicle speed.

TABLE OF CONTENTS

NOMENCLATURE

A	
A_W	Body cross section area
C	Body wetted area
C_D	Blade chord
C_{Da}	Drag coefficient $= DRAG/\frac{1}{2}\rho V_s^2 A$
C_{Df}	Appendage drag coefficient
C_{Dr}	Skin friction drag coefficient
C_{Du}	Discreet roughness drag coefficient
C_L	Unappended body drag coefficient
C_p	Blade section lift coefficient
C_P	Pressure Coefficient $= (p-p_o)/\frac{1}{2}\rho V_s^2$
	Power coefficient $= Q\omega/\frac{1}{2}\rho V_s^3\pi R^2$ for counterrotating propellers and SISUP $Q\omega = Q_F\omega_F + Q_A\omega_A$
C_Q	Torque coefficient $= Q/\frac{1}{2}\rho V_s^2\pi R^3$
C_T	Thrust coefficient $= T/\frac{1}{2}\rho V_s^2\pi R^2$
D	Propeller diameter
D_B	Body diameter
J	Advance ratio $= V_s/(RPS \cdot D)$
l	Length for non-dimensionalization
L	Length
L_B	Body length
p	Local static pressure in the wake
p_o	Free stream static pressure
Δp	Pressure jump through the blade
PC	Propulsive coefficient $= DRAG \cdot V_s/Q\omega$
Q	Propeller torque for counterrotating propellers and SISUP $Q = Q_F + Q_A$
r	Radial coordinate
r_{HUB}	Hub radius at the stacking line
R	Propeller radius
R_L	Reynolds number $= V_s L/\nu$
R_B	Body radius
T	Propeller thrust for counterrotating propellers and SISUP $T = T_F + T_A$
t	Blade section maximum thickness
u	Local velocity in the wake
V_P	Velocity from potential flow solution
V_s	Vehicle speed or free stream velocity
$\bar{x}$	Non-dimensional radial coordinate $= (r-r_{HUB})/(R-r_{HUB})$
y	Non-dimensional chordwise coordinate
z	Non-dimensional, normal distance from the body surface (i.e. z/l)
Γ	Bound circulation
ρ	Mass density of the fluid
σ	Cavitation index $= (p_o-p_{vapor})/\frac{1}{2}\rho V_s^2$
τ	Thrust deduction factor $1-\tau = DRAG/T$
ω	Propeller rotational rate
ν	Fluid viscosity

Subscripts

F - Forward propeller (or stator)
A - After propeller

INTRODUCTION

Except for those special applications where requirements dictate the use of counterrotating propellers, the choice between a single propeller and counterrotating propellers involves a tradeoff related to the higher efficiency of the counterrotating propellers and the greater complexity of the counterrotating machinery. Counterrotating propellers are more efficient for two reasons: (1) the thrust is divided between the two propellers so each propeller operates at a smaller thrust coefficient with corresponding lower induced drag of the blades; and (2) there is a net favorable effect of the interference velocities such that the tangential velocities generated by the forward propeller are removed by the after propeller consequently leaving less energy in the wake.

The second advantage of the counterrotating propeller system can be realized without counterrotating machinery by placing upstream of a propeller a stator that generates tangential velocities which are exactly canceled out by the propeller. The swirl inducing stator upstream of propeller (SISUP) concept is by no means a new idea; however, the counterrotating propeller design method developed at the Naval Ocean Systems Center (NOSC) provides a particularly good tool for comparing SISUP with conventional single and counterrotating propellers. All three types of propulsors may be considered counterrotating propellers where the single propeller is a counterrotating propeller with zero loading on the after propeller while SISUP is a counterrotating propeller with the forward propeller turning at zero RPM. Hence, all three propulsor types can be analyzed by the NOSC propeller design method yielding a truly equitable performance comparison. This paper will first report the results of a theoretical study which compares the performance of three propulsor types. Next, details of the design, manufacturing and at-sea testing of a SISUP propulsor will be presented.

THEORETICAL STUDY

Design Method

The design calculations described in the following sections were carried out using the wake-adapted, counterrotating propeller design method developed at NOSC and described in Nelson (7,8). This method treats the propeller blades as lifting surfaces and accounts for the vorticity in the wake wherein the propellers are operating. Recently, minor modifications to the method were made to rectify numerical problems associated with the forward propeller (stator) operating at zero RPM. It should be noted that the extensive nature of these calculations requires that they be made on a digital computer, and that the propeller design method has been used to design many counterrotating propeller sets all of which have met performance and cavitation requirements.

Propelled Vehicle

To make the performance comparison as realistic as possible an existing underwater vehicle was chosen as the body to be propelled by the three propulsor types. The vehicle used was one developed at the Naval Underwater Systems Center (NUSC) in Newport, Rhode Island. A major advantage in using this vehicle is that all of the data required for the propeller design was available. Wake and body drag measurements were made in a wind tunnel (Mautner, 6), and additional body drag measurements were made in a towing basin (West and Murray, 10). The afterbody geometry and location of the wind tunnel wake measurements are shown in figure 1. From the wind tunnel and towing basin drag data, the vehicle drag coefficient was determined to be C_D=0.114 for a vehicle speed of 40 knots in 55° seawater. This value of the drag coefficient was used throughout the theoretical study.

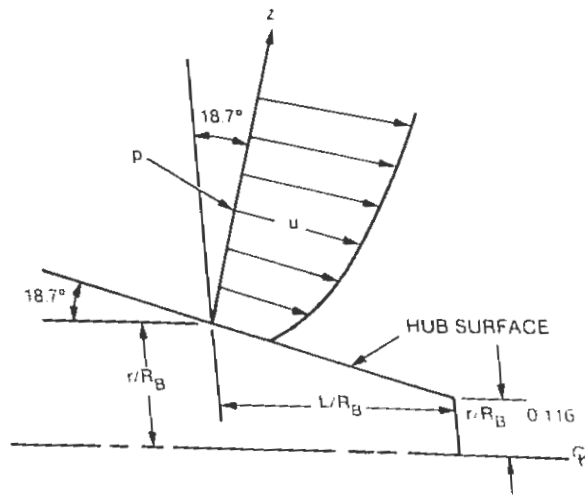

Figure 1. Physical Arrangement of the Boundary Layer Rake Measurements.

Blade Numbers

The number of blades used on the three propulsor types is given in table I. Except for the SISUP stator, the blade numbers were chosen on the basis of being typical of values used on actual designs. Moreover, the dependence of efficiency on blade number is weak, and no consideration was given to the harmonic content of the wake as that aspect of the propeller design was outside the scope of this study.

Propeller Type		Number of Blades
Counter-rotating	Forward	7
	After	5
SISUP	Stator	8
	Propeller	7
Single	Propeller	7

Table I. Blade Numbers

Special considerations entered into the choice of blade number for the SISUP stators because they operate in a local flow field rather than experiencing the circumferential mean due to rotation. The vehicle used in the study has identical cruciform fins, and the wake behind the fins is symmetrical about each fin position and repeats itself

every 90°. If tangential velocities in the wake are significant and each equally spaced stator blade is to see the same inflow, four stator blades must be used. However, if tangential velocities are negligible, eight stator blades, positioned as shown in figure 2, may be used while maintaining the same inflow to each blade. Since the measurement of tangential velocities was not a part of the wind tunnel test program (Mautner, 6), a blade number decision based upon the magnitude of the tangential velocities could not be made. Thus, it was assumed that the tangential velocities were negligible and eight stator blades were utilized. Whether or not the assumption is correct is not crucial as the stator blade design could be modified to compensate for the tangential velocities. The blades that are located 22.5° counterclockwise from the fins would have a slightly different pitch distribution from those located 22.5° clockwise from the fins.

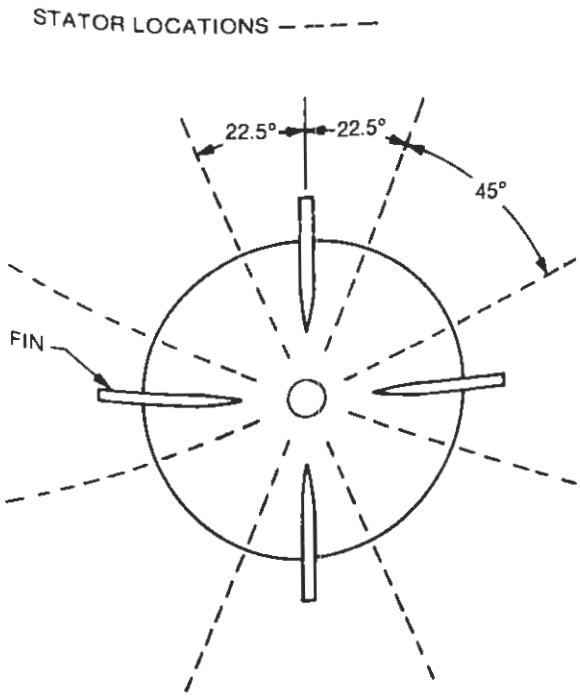

Figure 2. Allowable Stator Locations for a Boundary Layer With Negligible Tangential Velocities.

Inflow Data and Propeller Locations

The boundary layer or wake data consisting of inflow velocity and static pressure profiles were obtained at two axial locations on the test vehicle's afterbody. The circumferential mean profiles at the forward and after positions are presented in figures 3 and 4 respectively. Except for the SISUP stator, the propulsors were designed for operation in the flow described by these profiles. Since the stator blades are fixed they should not be designed using the circumferential mean velocities but should be designed using the local inflow. From the wind tunnel wake data, the inflow velocity profile at the stator locations (±22.5° from the fins) was constructed and is shown in figure 3. Since the circumferential variation of static pressure is slight, the circumferential mean profile given in figure 3 was used for the stator.

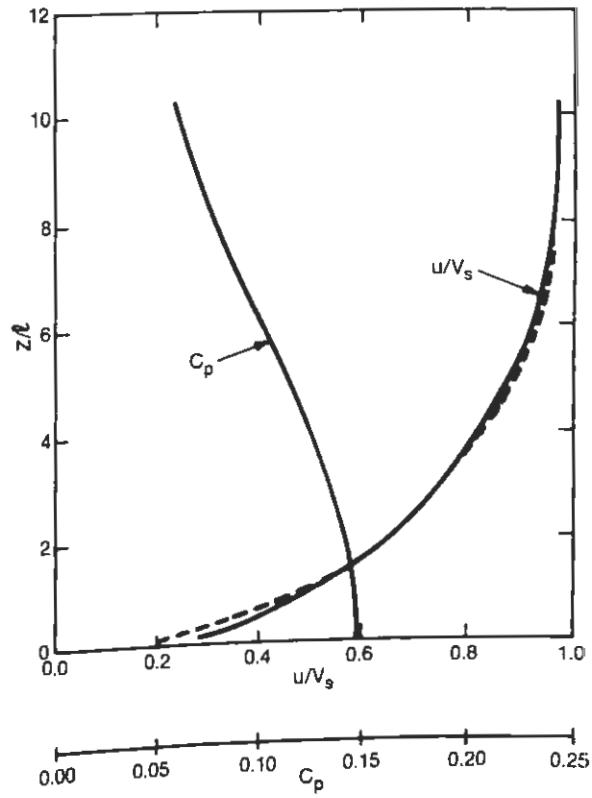

Figure 3. Circumferential Mean Inflow Velocity and Static Pressure Profiles at the Forward Wake Measurement Location. C_p - ▬ Stator and Propeller; u/V_s - ---- Stator, and ▬ Propeller.

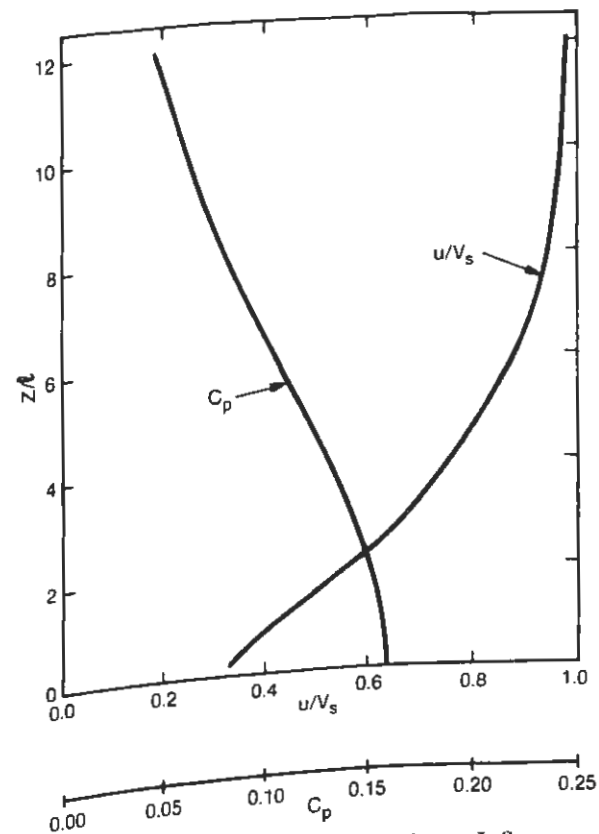

Figure 4. Circumferential Mean Inflow Velocity and Static Pressure Profiles at the Aft Wake Measurement Location.

The axial locations of the blading systems were made to correspond to the positions of the wake measurements (figure 1). For the counterrotating propellers and SISUP, the forward propeller (or stator) was located at the position of the forward wake measurements while the after propeller was located at the position of the after measurements. For convenience and to eliminate the need to analytically determine profiles at another position, the single propeller was located at the position of the after wake measurements. If a single propeller were actually used on the vehicle it probably would not be located at that position. However, the dependence of efficiency on axial position is weak so the precise location used in the performance comparison is not of great importance.

Loading Distributions

The spanwise or radial distribution of load on the blades is controlled by the radial distribution of bound circulation. The bound circulation distributions used in the performance comparison study are shown in figure 5. The distribution used on the forward propeller or stator has two notable features: (1) it does not drop to zero at the hub but is maintained at one half its maximum value; and (2) the distribution is inflected near the tip to unload this region. The circulation distribution at the after propeller is determined by the requirement of tangential velocity cancellation along each streamline. The single propeller circulation distribution is modified at the inner radii to achieve zero circulation at the hub. This modification is necessary to reduce the possibility of a strong hub vortex since no mechanism exists with a single propeller for tangential velocity cancellation.

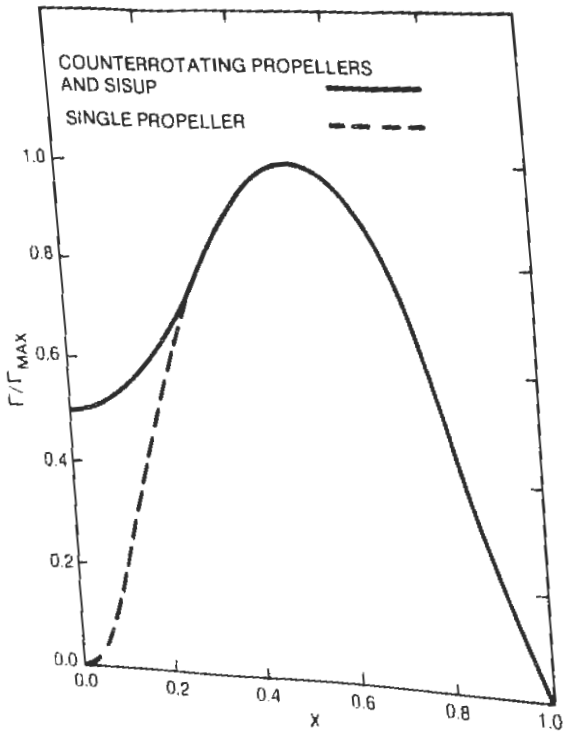

Figure 5. Radial Distribution of Bound Circulation.

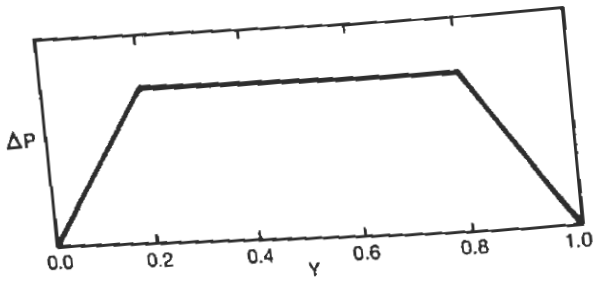

Figure 6. Chordwise Load Distribution.

Figure 6 illustrates the chordwise loading distribution used in the performance calculations. A trapezoidal distribution of this type unloads the leading edge. Hence, the off-design angle-of-attack loading associated with operation in a circumferentially varying wake added to the steady loading is greatly reduced in the critical leading edge region.

Blade Thickness

All of the blade section thickness profiles were developed from the NACA 0010-64 section, and the detailed procedure for developing the sections can be found in Nelson (7,8). Figure 7 presents the radial distribution of thickness-to-chord, t/C, used throughout the performance calculations. The t/C distribution increases rapidly near the hub with the purpose of providing adequate structural strength; however, whether or not this particular t/C distribution is adequate for all cases investigated is not known since detailed stress calculations were not performed. Nevertheless, the moderate changes in blade geometry near the hub that might be required for structural reasons would have a small effect on performance.

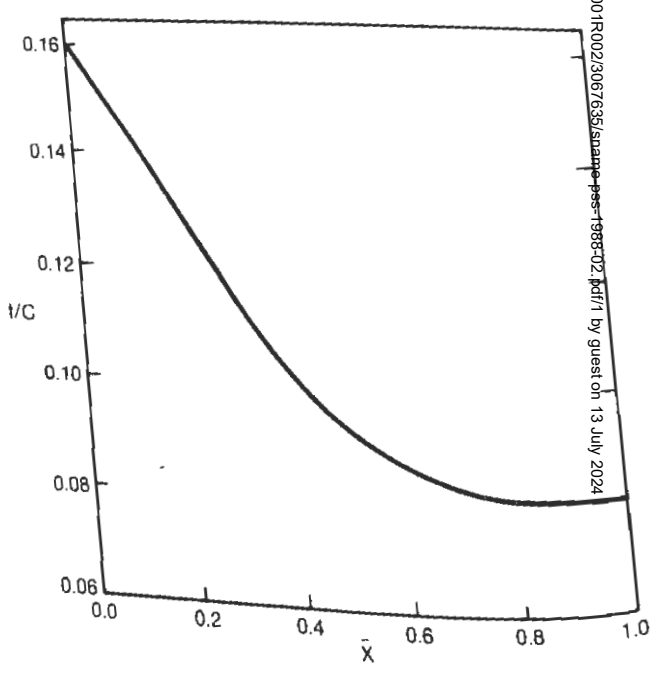

Figure 7. Radial Distribution of Thickness-to-Chord Ratio.

Cavitation Calculations and Blade Chord

To put the performance comparison on a common basis, all calculations were carried out holding the resistance to blade surface cavitation a constant. This was accomplished in the following manner. First, the radial distribution of $(C/D)_{MIN}$ (the minimum value of C/D that satisfied the cavitation criterion) was calculated. The actual chord-to-diameter ratio distribution was then fit around the $(C/D)_{MIN}$ curve as illustrated in figure 8. A blade having constant chord over the inner portion was chosen for the sake of simplicity, and a blade surface cavitation index of σ=0.85 was used in the calculation of $(C/D)_{MIN}$. This value of cavitation index was chosen based upon no special consideration but is merely a reasonable value for a vehicle of the type used in this study.

It was found that the method described above for determining blade chord based upon cavitation resistance was unsatisfactory for the SISUP stator because it resulted in excessively large blade section lift coefficients. For the stator blades, the maximum value of C/D was increased sufficiently to yield a maximum blade section lift coefficient of 0.8 at the blade root.

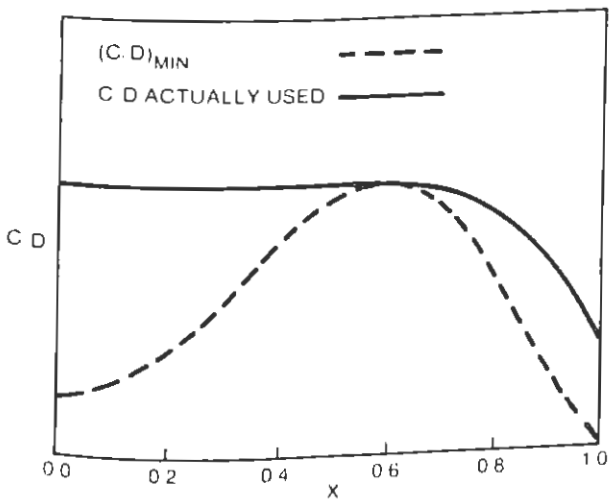

Figure 8. Typical Radial Distribution of Chord-to-Diameter Ratio (actual C/D values are design dependent).

Theoretical Results

The results of the performance calculations are presented in figure 9 where, for each of the three propulsors, the variation of propulsive coefficient with both radius and RPM is shown. Since propulsors of radius greater than the body radius are not of practical interest, the study was limited to radii only slightly larger than the body radius. In performing the computations only enough points were calculated to determine the optimum radius (the radius at which PC is a maximum). Valid solutions that satisfy the cavitation criterion may exist off either end of the curves in figure 9. The minimum RPM's investigated correspoud to cases which optimize near the body radius while the maximum RPM's investigated lie close to the upper limit at which the cavitation criteria can be met. In particular, a sufficient number of solutions to establish the optimum radius could not be found for counterrotating propellers, SISUP and single propeller at RPM's of 1900, 1700 and 1900 respectively.

A significant observation from figure 9 is that, using the single propeller as a base line, the increase in efficiency for SISUP is greater than 50% of that achieved by counterrotating propellers. This is a very favorable result considering the fact that counterrotating machinery is not required. Another interesting observation is that, at a given RPM, SISUP optimizes at a smaller radius than the single propeller but at a larger radius than the counterrotating propellers.

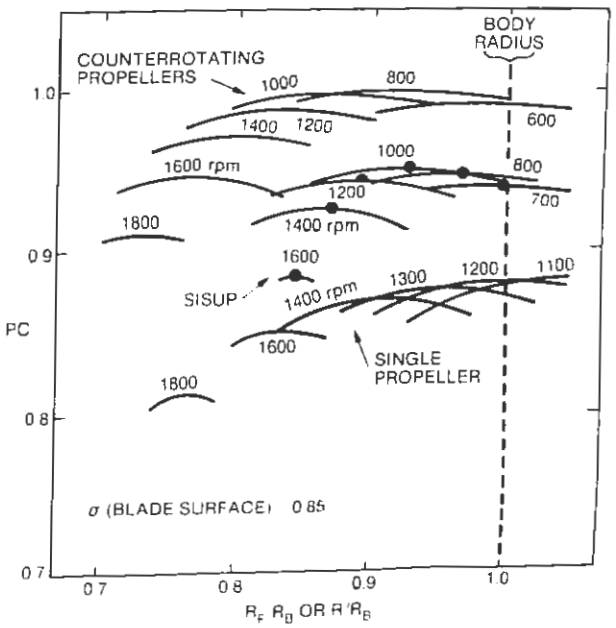

Figure 9. Theoretical Performance Comparison of Three Propulsor Types on the Test Vehicle.

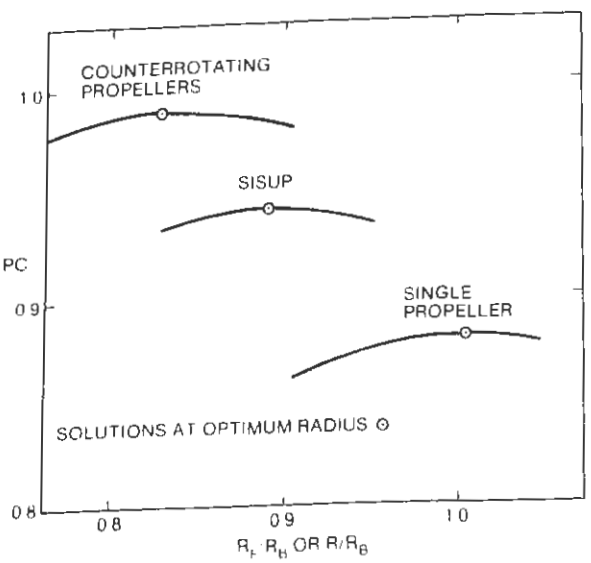

Figure 10. Performance Comparison at 1200 RPM.

To provide more detailed information, a comparison of the three propulsors was made at 1200 RPM, and the results are presented in figure 10. Solutions at the optimum propulsor radius were obtained, and, from these solutions, a detailed comparison of propulsive and geometric characteristics of the three propulsor types is given in table II.

SISUP DESIGN, MANUFACTURING AND TESTING

The encouraging results obtained from the above study prompted further investigation of SISUP. The work described below was conducted with the purpose of demonstrating the feasibility of using a SISUP propulsor by designing and fabricating such a propulsor for testing on a NOSC research vehicle. The remainder of the paper will describe the design, manufacturing and at-sea testing of a SISUP propulsor which includes discussion of the design specifications, input profiles, a parametric study and final design characteristics.

Design Specifications and Input Profiles

The general propulsor design guide lines were established to provide a propulsor which, in addition to its single rotation simplicity, would also be capable of providing speeds greater than the 40 knots used in the theoretical study. The general SISUP design guidelines are as follows: (a) a vehicle speed of 55 knots; (b) a blade surface cavitation index of $\sigma = 0.8$; and (c) the design RPM and diameter will be determined by efficiency and space requirements.

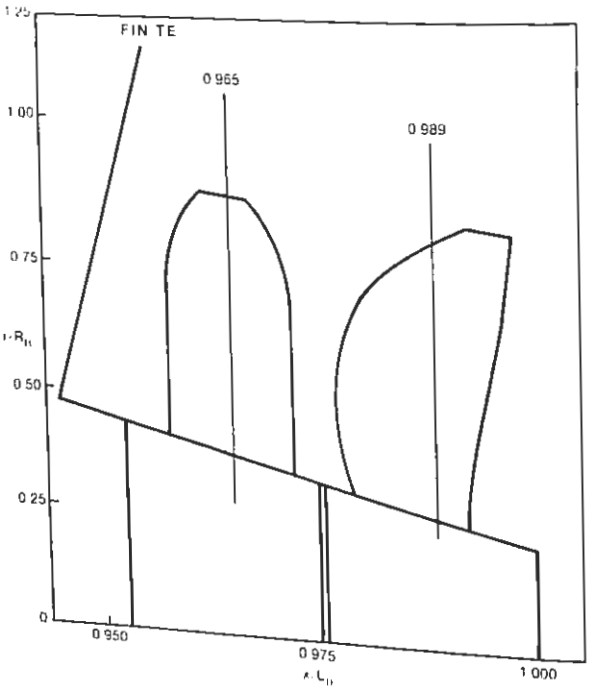

Figure 11. Afterbody Geometry and Swept Volume of the SISUP Propulsor.

Parameter	Counterrotating Propellers		SISUP		Single Propeller
Propulsive Coefficient - PC	0.9881		0.9415		0.8797
Thrust Deduction - $1-t$	0.8695		0.8750		0.9013
Power Coefficient - C_P	0.1680		0.1528		0.1284
Thrust Coefficient - C_T	0.1909		0.1644		0.1253
Torque Ratio - Q_A/Q_F	1.000		1.000		---
Thrust Ratio - T_A/T_F	1.030		-7.604		---
	Fwd Prop	Aft Prop	Stator	Prop	Prop
Propeller Radius R/R_B or R_F/R_B	0.828	0.758	0.890	0.825	1.005
Advance Ratio - J	2.328	2.546	---	2.339	1.920
Maximum Lift Coefficient - $(C_L)_{MAX}$	0.5035	0.5021	0.7941	0.3836	0.3931
Maximum Chord-to-Diameter Ratio - $(C/D)_{MAX}$	0.1073	0.1683	0.2196	0.2587	0.1429

Table II. Comparison of Propulsive and Geometric Characteristics of Optimum Propulsors at 1200 RPM.

In addition to the above specifications, the stacking lines for the stator and propeller were chosen to correspond to the location of the measured inflow profiles obtained during wind tunnel tests (Franco, 1; Kontos, 4). The afterbody geometry and stacking line locations are shown in figure 11, and the measured inflow velocity, u/V_s, and static pressure coefficient, C_p, profiles at the stator and propeller locations are given in figure 12 and 13.

In order to perform thrust deduction calculations, the potential flow velocity profiles, V_p/V_s, at the stator and propeller are required. The three-dimensional body and appendage coordinates and off-body points for the research vehicle were computed using the program described in Mautner (5). Next, the potential flow pressure distribution along the body and the potential flow velocity profiles at the stacking lines were calculated using the Douglas three-dimensional potential flow program (Hess and Smith, 2 and 3). The resulting circumferentially averaged potential flow profiles, at the stacking line locations, are given in figure 14.

The above mentioned profiles were supplemented with the following design criteria: (a) the radial distribution of bound circulation (Γ/Γ_{max}) for the stator is that shown in figure 5 (with $\Gamma \neq 0$ at $\bar{x}=0$); (b) the thickness-to-chord (t/C) distribution for the stator and propeller is shown in figure 15; (c) the chord-to-diameter (C/D) ratio profiles were calculated for each design iteration to satisfy both stress (blade modeled as a simple beam) and cavitation requirements; (d) the chord-to-diameter profiles were specified to have

for the stator $\dfrac{(C/D)_{root}}{(C/D)_{max}} = 1.00 \quad \dfrac{(C/D)_{tip}}{(C/D)_{max}} = 0.40$

and the propeller $\dfrac{(C/D)_{root}}{(C/D)_{max}} = 0.75 \quad \dfrac{(C/D)_{tip}}{(C/D)_{max}} = 0.40$

(e) the propulsor has 8 stator blades and 7 propeller blades; and (f) calculation of the body drag was based on wind tunnel tests (Franco, 1; Kontos, 4) and was analytically extrapolated to full scale. The vehicle drag coefficient is $C_D=0.0997$.

Parametric Study

With the specification of the input design data complete, a parametric study was performed (using the propeller design procedures described in Nelson (7,8)) to determine the relationship between propulsive coefficient, PC, propeller diameter, D, and RPM while holding the cavitation index, $\sigma=0.8$, constant. During each design iteration, the radial distributions of the chord-to-diameter ratio, C/D, which satisfied both blade surface cavitation and stress level requirements were calculated. The cavitation requirement was the determining factor for all stator and propeller C/D profiles except for the stator with $R_F/R_B = 0.94$. The results of the parametric study are shown in figure 16 and indicate that the optimum SISUP configuration occurs in the neighborhood of $R_F/R_B = 0.9$ for the stator and an RPM range of 2400 - 2800.

In order to utilize existing hardware (with minimum modifications), gear box output speeds of 2665 and 2831 RPM were used in a more detailed analysis of the variation of propulsive coefficient with stator diameter. The results are given in figure

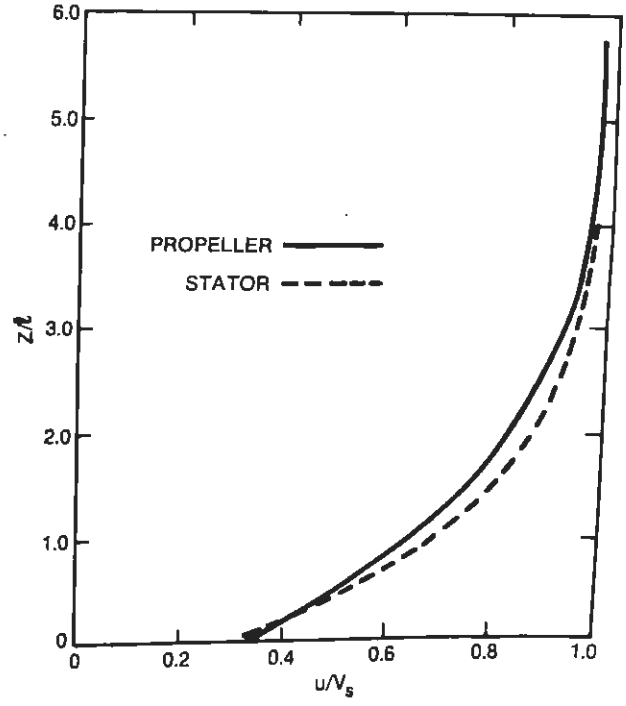

Figure 12. Inflow Velocity Profile at the Stator and Propeller Location.

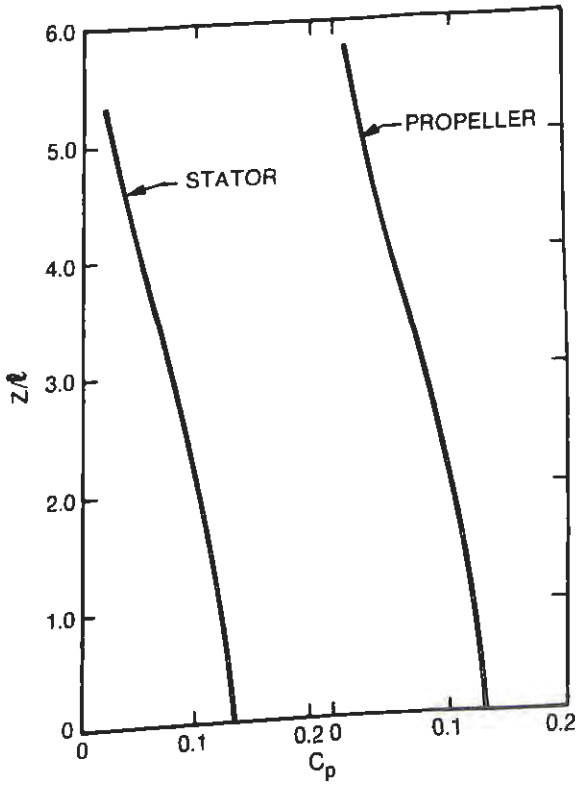

Figure 13. Static Pressure Profile at the Stator and Propeller Location.

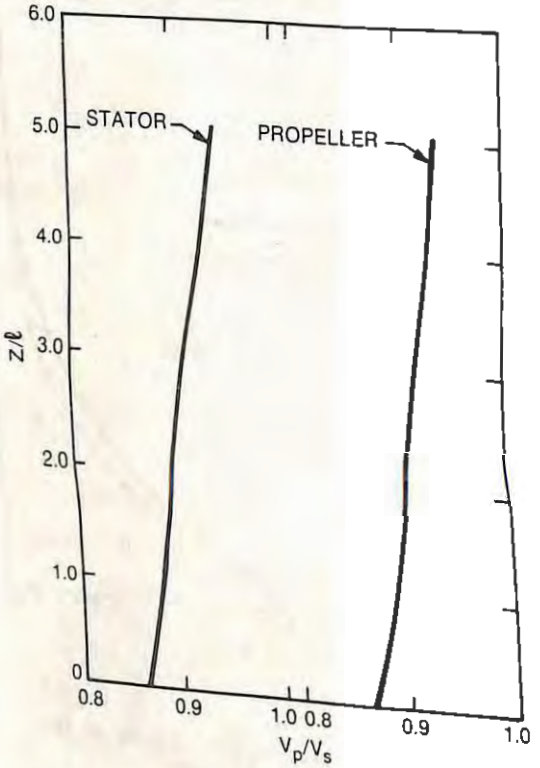

Figure 14. Circumferential Mean Inflow Velocity Profile at the Stator and Propeller Location From a Potential Flow Solution.

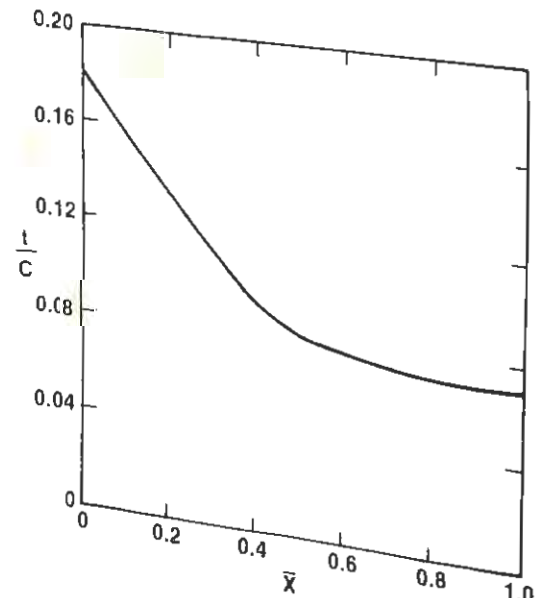

Figure 15. Thickness-to-Chord Distribution on the Stator and Propeller.

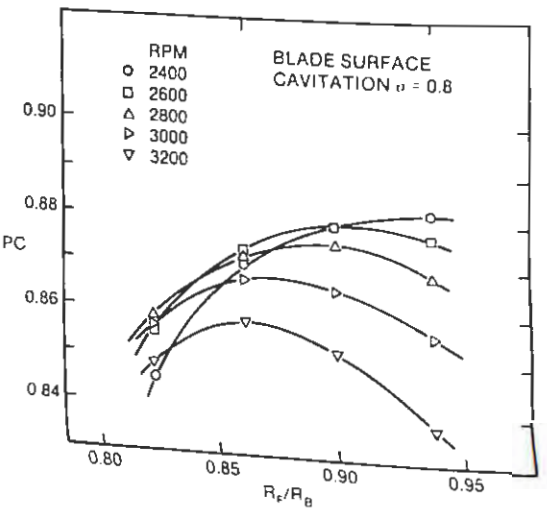

Figure 16. Variation of Propulsive Coefficient with Stator Diameter.

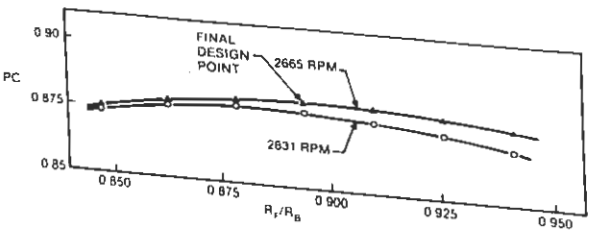

Figure 17. Variation of Propulsive Coefficient with Stator Diameter for Determination of Final Design Point.

17, and it can be seen that the optimum point, for both RPM's, occurs at $R_F/R_B = 0.894$. The 2665 RPM case was chosen as the final design point due to the slightly higher performance and the lower blade tip speed.

Final Design

The final design procedure for the SISUP propulsor ineluded the specification of a skew distribution, detailed stress level cheeks and the calculation of final blade geometry and performance characteristics. The skew distrihution chosen for the propeller was based on past experience and is somewhat arbitrary since the circumferential variation of the wake was not available for the harmonic analysis required to calculate the skew distribution. Additionally, the amount of skew was restricted by the fact that the trailing edge of the propeller could not extend beyond the aft face of the hub. The propeller was designed with a 45 degree leading edge skew, and the stator blades were not skewed. The blade stresses for the stator and propeller were calculated using the NASTRAN stress analysis program where the blades were modeled using 40 elements of the 20-point isoparametric type.

Vehicle Velocity - V_s (knots)	55
Drag Coefficient - C_D	0.0997
Propulsive Coefficient - PC	0.881
Thrust deduction - $1-\tau$	0.896
Torque Ratio - Q_A/Q_F	1.0
Blade Surface Cavitation - σ	0.8

Parameter	Stator	Propeller
Blade Number	8	7
R/R_B	0.894	0.838
RPM	----	2665
Advance Ratio - J	----	2.35
Maximum C/D	0.145	0.253
t/C At The Hub	0.18	0.18
t/C At The Tip	0.07	0.07
Max Principal Stress (psi)	16335	21143
Maximum C_L	0.798	0.417
Leading Edge Skew (deg)	----	45

Table III. Summary of SISUP Final Design Calculations

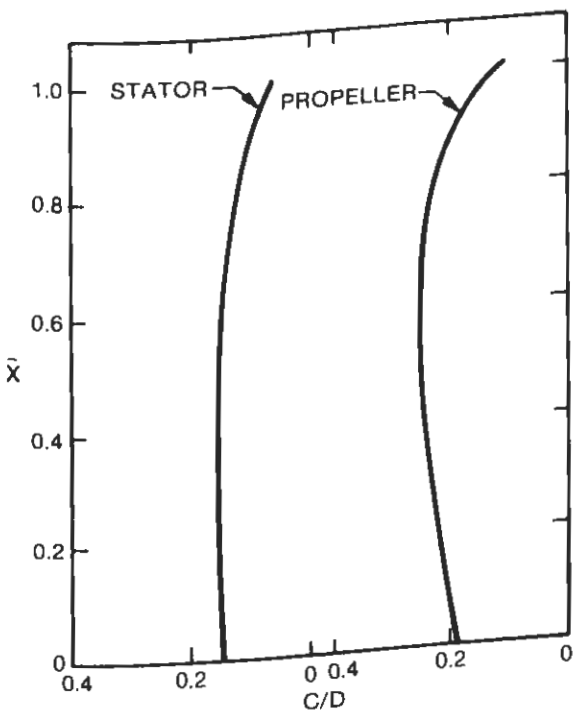

Figure 18. Final Design Chord-to-Diameter Distribution on the Stator and Propeller.

The final design summary for the SISUP propulsor is given in table III, and the final design, chord-to-diameter profiles are shown in figure 18. The swept area in the meridian plane for the stator and propeller is shown in figure 11. An interesting comparison can be made between the SISUP characteristics determined in the theoretical study and those associated with the current design. The comparison, given in table IV, shows that even though the two vehicles have significantly different length scales, the SISUP propulsor characteristics and performance values are approximately the same. A significant difference is found in the maximum C/D for the two stators where the approximate 34% reduction in maximum C/D for the current design is due to specification of a more appropriate value based on calculated stress levels. Also, the RPM's of the two SISUP propellers are significantly different (factor of ≈ 2.2), however, the advance ratios for the two propulsors are nearly equal.

Manufacturing

Both the stator and propeller were manufactured in the NOSC machine shop using numerical milling machines. The stator was manufactured by milling each stator blade and then inserting the blades into the hub. This technique allows the stator blades to be rotated $\pm 5°$ from their design location. If necessary, rotation of the stator blades can be used to improve the propulsor's torque balance during both engine start up and normal operation.

The propeller was machined from a solid billet. The manufacturing process starts with the solid billet being machined on a tracer lathe using a template to produce the swept volume of the propeller. Next, the billet is roughly machined to produce crude blade shapes. Machining of the propeller blades is done at a constant percentage of chord which provides smooth leading and trailing edges as well as a better blade/hub juncture. Final fabrication begins with roughing cuts and ends with finishing cuts as fine as 0.125 mm (0.005 in) to insure that there is no blade movement during machining. After machining, both the stator and propeller were hand finished, inspected and anodized. The SISUP propulsor is shown in figure 19.

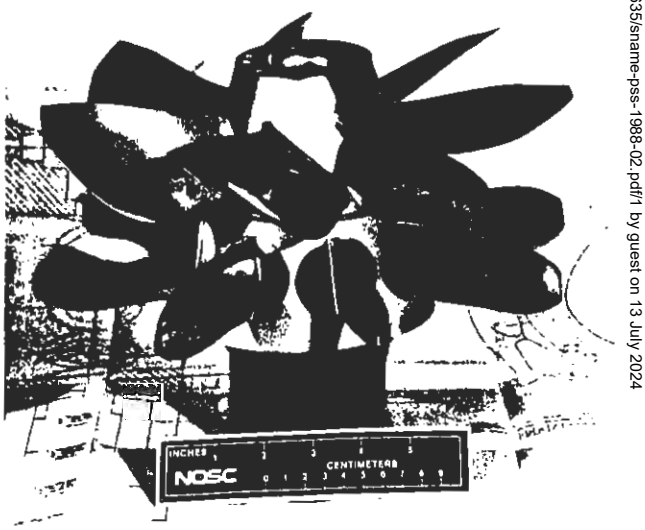

Figure 19. The SISUP Propulsor Hardware.

Parameter	SISUP from Theoretical Study		SISUP Current Design	
Vehicle Speed - V_s (knots)	40		55	
Drag Coefficient - C_D	0.114		0.0997	
Cavitation Index - σ	0.85		0.80	
Vehicle L_B/D_B Ratio	11.8		8.7	
Propulsive Coefficient - PC	0.9415		0.881	
Thrust Deduction - $1-\tau$	0.8750		0.896	
Power Coefficient - C_P	0.1528		0.1575	
Thrust Coefficient - C_T	0.1644		0.1358	
Torque Ratio - Q_A/Q_F	1.000		1.000	
	Stator	Prop	Stator	Prop
Blade Number	8	7	8	7
Propeller Radius R_F/R_B	0.890	0.825	0.894	0.838
RPM	---	1200	---	2665
Advance Ratio - J	---	2.339	---	2.35
Maximum Lift Coefficient - $(C_L)_{MAX}$	0.794	0.384	0.798	0.417
Maximum Chord-to-Diameter Ratio - $(C/D)_{MAX}$	0.2196	0.2587	0.145	0.253
Thickness-to-Chord Ratio - $(t/C)_{HUB}$	0.16	0.16	0.18	0.18
Thickness-to-Chord Ratio - $(t/C)_{TIP}$	0.08	0.08	0.07	0.07

Table IV. Comparison of Propulsive and Geometric Characteristics of Two SISUP Propulsors.

Test Vehicle and Power Plant

The geometry of the test vehicle is consistent with the vehicle used during the wind tunnel tests to determine the body drag and the wake data. In order to provide single rotation for the SISUP propulsor, a counterrotating torpedo engine was modified to operate in the single rotation mode. Hardware modifications were necessary to adapt the engine to the vehicle's afterbody, and sensors to measure RPM, torque and vehicle speed were installed.

In a standard counterrotating propulsion unit, the engine crankcase is mounted on a bearing and allowed to rotate with the outer shaft, and it is the rotation of the crankcase which drives the fuel pump, water pump and alternator. In order to provide single rotation, provisions had to be made to run the accessories off the inner shaft since the outer shaft and crankcase would be constrained from rotating. The accessories were placed aft of the engine and geared directly to the inner shaft. Also, due to space limitations, the alternator was removed, and vehicle power was supplied by a 40-volt battery pack located in the nose section of the vehicle. Two shell sections, with a combined length of 45.7 cm (18 in), served to lengthen the afterbody thus providing the additional space required by the powerplant.

As mentioned above, sensors were added to the test vehicle to provide the data required to estimate propulsion performance. To measure vehicle speed, a pitot-static tube was mounted approximately 38.1 cm (15 in) from the nose. In addition to the digital tachometer used to measure RPM and the load cell to measure torque, the vehicle heading, depth and fin splay were recorded. The vehicle's guidance logic was programmed to execute a "race track" geometry at a depth of approximately 38 m (125 ft).

All sensors were calibrated before and after the at-sea tests, and static tests of the power plant were made. Bench tests were made to determine (a) the torque required to drive the fuel and water pumps, (b) the torque due to gear and bearing friction and (c) the inner shaft o-ring friction. The total torque loss due to accessories and friction was measured to be 1.58 kg-m (11.4 ft-lbs).

Sea Run Results and Discussion

The SISUP propulsor was tested off the coast of San Diego, California. The vehicle was launched using a slide launcher and executed a "race track" geometry. No problems were associated with this test, and the resulting data forms the basis of the propulsion estimates and subsequent comparison design predictions. The results are presented in table V. It should be noted that while only a small length difference exists between the design and test vehicle, the vehicle speed and RPM during the at-sea test was nominally 33 knots and 1590 RPM as compared to the design values of 55 knots and 2665 RPM.

The first step taken in estimating the performance of the SISUP propulsor was adjustment of the vehicle drag to account for differences in vehicle velocity and length. The vehicle drag coefficient can be expressed as

$$C_D = C_{Du} + C_{Df} + C_{Da} + C_{Dr} \qquad (1)$$

where $C_{Dr} \approx 0.00318$ for the discrete roughness has been previously estimated for similar vehicle hardware and the C_{Da}=0.0084 for appendage drag (from wind tunnel tests) is considered approximately independent of Reynolds number. The unappended vehicle drag coefficient was obtained from wind tunnel tests and has a value of $C_{Du} = 0.08726$ for a vehicle length of 289.6 cm (114 in) and a speed of 40 knots. The drag coefficient will be modified by computation of the differences in skin friction drag at the wind tunnel test speed and the at-sea measured vehicle velocity of 33.3 knots. The skin friction drag is computed using (see equation 21.16a, Schlichting, 9)

$$C_{Df} = \frac{0.455}{(\log R_L)^{2.58}} \cdot \frac{A_W}{A} \qquad (2)$$

which yields a difference in skin friction drag coefficient, for the two body lengths, of C_{Df}=+0.0034 and a total vehicle drag coefficient of $C_D = 0.1022$ at the test velocity of 33.3 knots.

The range of values presented in table V for the at-sea measurements reflect the uncertainties induced by the calibration shifts between pre-run and post-run calibrations. Uncertainties from the following sources were not included in the data analysis: a) instrumentation error bands; b) estimation of discrete roughness drag coefficient; c) pitot-static tube errors; and d) extrapolation of wind tunnel data to sea run Reynolds numbers.

A direct comparison of the measured and design values of propulsive coefficient and advance ratio are not valid because the test vehicle was not operated at the design vehicle velocity. However, since both the propulsive coefficient and advance ratio are weak functions of vehicle velocity, approximate agreement of measured and design values should occur if the propulsor is operating correctly. The good agreement of the design and sea run data given in table 5 confirms satisfactory operation of the propulsor.

It should be noted that the SISUP propulsor was designed using a vehicle for which only unappended inflow velocity and static pressure profiles were available. Since the appendages significantly affect both the circumferential variation and the circumferential mean inflow velocities, neither the stator nor the propeller were designed for the precisely correct inflow. This fact may account for not obtaining a completely satisfactory torque balance, Q_A/Q_F, as indicated by the approximate $\pm 3^\circ$ rudder splay during the straight portion of the test run. Finally, it should be mentioned that no excessive vehicle roll was experienced due to torque imbalance during propulsor start up (i.e. $Q_A >> Q_F$ at low RPM and V_s).

CONCLUSIONS

The theoretical study demonstrated that, using the single propeller as a base line, the increase in efficiency for SISUP is greater than 50% of that achieved by counterrotating propellers. Since SISUP does not require counterrotating machinery, the predicted efficiency payoff for use of SISUP's single rotation system is very high as compared to that of a single propeller.

The excellent results obtained in the theoretical study prompted the design, manufacturing and at-sea testing of a SISUP propulsor on a research vehicle. The comparison of at-sea and design values shows good agreement with sea run values of PC=0.886-0.915 at a estimated full scale

Parameter	Design	At-Sea Data
V_s (knots)	55	33.3 (55.7)
L_B (in)	111.4	113.8
C_D	0.0997	0.1022
RPM	2665	1580 - 1606 (2630)
J	2.35	2.36 - 2.40
PC	0.881	0.886 - 0.915
C_Q	0.118	0.122 - 0.123
C_P	0.315	0.318 - 0.329
( ) represents full scale estimates		

Table V. Comparison of SISUP Design and At-Sea Test Results

speed of 55.3-56.2 knots as compared to the design predictions of PC=0.881 and V_s=55 knots. The satisfactory performance of this SISUP propulsor indicates its potential use as a propulsor for applications where single rotation, instead of counterrotation, is desired or required.

ACKNOWLEDGMENTS

The theoretical study was funded by the Torpedo Hydromechanics and Hydroacoustics program of the Naval Sea Systems Command. The SISUP design, fabrication and testing were supported by the Naval Ocean Systems Center Independent Exploratory Development Program.

REFERENCES

1. B. G. Franco, "Data Report of a Full Scale Torpedo Force Model Low Speed Wind Tunnel Test for the U.S. Naval Ordnance Test Station," Northrop Corporation, Norair Division Report NRL-A-763, 1967.

2. J. L. Hess and A. M. O. Smith, "Calculation of Nonlifting Potential Flow about Arbitrary Three-Dimensional Bodies," Douglas Aircraft Company Report ES40622, 1962.

3. J. L. Hess and A. M. O. Smith, "Calculation of Potential Flow About Arbitrary Bodies," Progress in Aeronautical Sciences Series, Vol. 8, Pergamon Press, 1966.

4. E. G. Kontos, "Data Report of the Pressure Coefficients on the Afterbody of The Naval Underwater Warfare Center (NUWC) Configuration B Torpedo Measured in a Low Speed Wind Tunnel Test," Northrop Corporation, Norair Division Report NRL-A-831, 1968.

5. T. S. Mautner, "A Computer Program Package for Providing Input to the Douglas Three-Dimensional Potential Flow Program: A User's Manual," NOSC, TR 352, 1978.

6. T. S. Mautner, "An Optimization Method for the Reduction of Unsteady Propeller Forces," AIAA Paper No. 88-0265, Reno, NV, 1988.

7. D. M. Nelson, "A Computer Program Package for Designing Wake-Adapted Counterrotating Propellers: A User's Manual," NUC TP 494, 1975.

8. D. M. Nelson, "Development and Application of a Lifting Surface Design Method for Counterrotating Propellers," NUC TP 326, 1972.

9. H. Schlichting, Boundary Layer Theory, 6th ed., McGraw-Hill Book Co.,New York, 1968.

10. E. E. West, and L. O. Murray, "Powering Predictions for a Quiet Experimental Vehicle Designated NSRDC Model 5310," NSRDC Report 120-H-08, 1973